OCEAN APPLICATIONS TECHNICAL NOTE 18

Momentum Fluxes in the Bryan - Cox Ocean Circulation Model

by

M. J. Bell

Met Office
FitzRoy Road, Exeter, Devon. EX1 3PB

1. Introduction

There are now several ocean general circulation models with active groups of users (e.g. Bleck & Chassignet 1994, Blumberg & Mellor 1987). The Cox model (Bryan 1969 and Cox 1984) is, however, probably still the most widely used by deep ocean circulation modellers and the most well established.

The Cox model divides its horizontal velocities into a barotropic part, which does not vary with depth, and a baroclinic part defined by the condition that its vertical average is zero at each grid point. In the standard version of the Cox code the barotropoic flow is non-divergent and is represented by a streamfunction. The arrangement of the grid point values of the tracers and the main velocities (which advect the tracers) in this model is that of the B-grid (Arakawa & Lamb 1977) in the horizontal and the Lorenz grid in the vertical (see section 2 for more details). A second set of velocities is defined on the faces of the velocity cells and used to advect the main velocities. This second set of velocities, which will be referred to as the face velocities, is derived from the baroclinic and barotropic velocities on the main grid but is not a simple linear interpolation or average of those velocities. The model represents the ocean's bathymetry by a series of steps. Face velocities directed normal to the bathymetry are located half a grid square in from the land boundary and used to advect momentum.

Figure 1a displays some zonal velocity profiles from a model integration on a global 1° grid (which is described in section 8) in the region of the Gulf Stream, where there are steep steps in the bathymetry. The continuous line shows the zonal velocity on the main grid at 283 °E, 32.5 °N and the line with diamonds the zonal velocity at the next main grid point to the east. The model is 240 metres deep (9 levels) at the western of these two points and 800 metres deep (12 levels) at the eastern point. The line with asterisks indicates the mean of these two velocities, which is the linear interpolation of the velocities from the main grid onto the face velocity point at 283.5 °E, 32.5 °N. The face velocities at the same point as calculated by the original Cox code are indicated by the line marked with plus symbols. It is clear that these two calculations of the face velocities do not agree well above or below the bathymetric step. It is worth noting that the vertical shears of the two profiles agree except between 200 m and 300 m, i.e. in the layer containing the top of the bathymetric step.

Figure 1b provides an example of the differences between the zonal face velocity at 289.5 °E, 37.5 °N and velocities from the surrounding main velocity gridpoints. Here the model is 3040 metres deep (16 levels) at the western gridpoint and 3650 metres deep (17 levels) at the eastern gridpoint. Velocities are only shown below 1500 m depth. The main velocity field varies little with depth whilst the face velocity increases by more than 2.8 cm/s at the bathymetric step.

The main purpose of this paper is to explain why the main and face velocity fields do not agree over bathymetric steps and to consider the merits of the original and of alternative formulations for the face velocities.

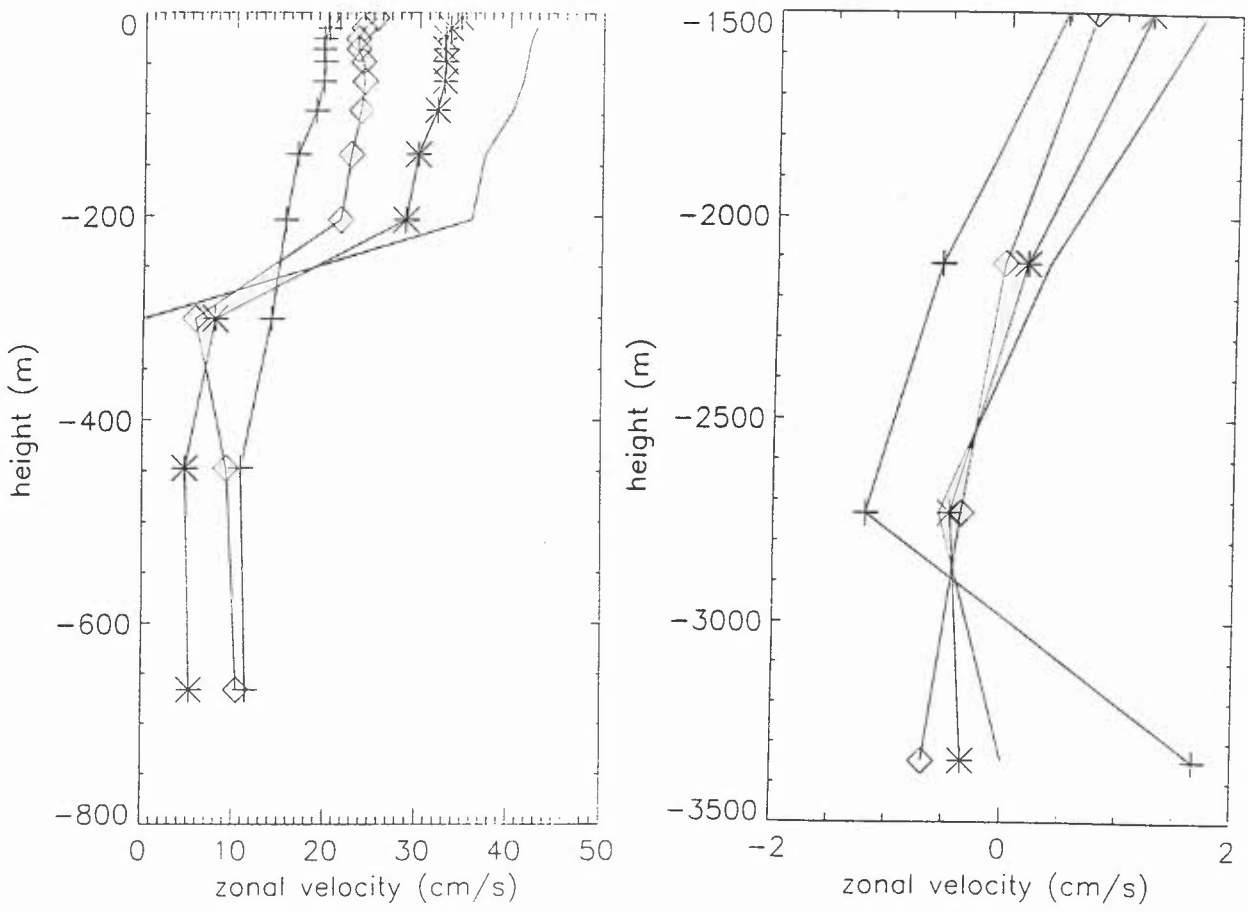

(a) **(b)**

Figure 1: Zonal velocities (cm/s) as a function of height (m) at grid points straddling a step in the bathymetry. ----- is the velocity on the main grid at the western gridpoint; -✧-✧- is the velocity one grid point to the east; -*-*- is the linear interpolation of these velocities to the face velocity point; -+-+- is the face velocity calculated by the original Cox scheme. Symbols indicate actual model values. (a) is at a point in the Gulf Stream, where the western point is 240 m deep and the eastern point 800 m deep (b) is centred at 289.5 °E, 37.5 °N where the western point is 3040 m deep and the eastern one 3650 m deep and only displays velocities below 1500 m depth.

The main reason for paying attention to vertical velocities in ocean models is because of the importance of vortex stretching in potential vorticity conservation. The vorticity in the Cox model is calculated on the tracer grid. It is the bottom vertical velocity on the tracer grid, not the velocity grid, which determines the vortex stretching (Bell 1997). The results presented in section 8 and Webb (1995) show that in a **coarse** grid model the tracer fields are not particularly sensitive to the momentum fluxes. These points explain in large part how Cox models could use a very poor formulation of the momentum fluxes without serious repercussions.

Section 2 describes the layout of the grid and the notation used in this paper (which follows that of Cox 1984). Section 3 provides more details on the results presented in figure 1 and explains why the main and face velocity fields do not agree and are inconsistent. Section 4 defines five alternative formulations (A-E; A being the original Cox formulation and E Webb's 1995 scheme) for the face velocities. A list of desirable properties by which these formulations can be judged is suggested in section 5. Section 6 derives and discusses each of the properties for each scheme. Table 4 (in the concluding section) indicates which properties are satisfied by each scheme. Webb (1995) drew attention to the influence of noise in the thermal field on the vertical velocities calculated using the original scheme. Section 7 presents simple calculations which estimate the noise in the velocity fields arising from grid-scale noise typically present in the streamfunction and thermal fields. These guide the discussion in section 8 of results on the horizontal and vertial velocities from short integrations of a 1° global model using the various schemes. Section 9 summarises the main conclusions.

2. Cox grid and notation

Figure 2 illustrates the arrangement of the variables on the grid used by the Cox model. Figure 2a is a vertical section (λ, z plane) and figure 2b is a horizontal section (λ , ϕ plane); ϕ is latitude, λ is longitude and z is the vertical ordinate (which increases in the upward direction).

In the horizontal (figure 2b) the tracer values are stored at the points marked T and both horizontal components of velocity (u,v) at the points marked X; u is eastward and v northward velocity. The face velocities on the velocity cell faces are (u*,v*). The eastward flux into each velocity cell is calculated at the west (and east) face points marked □ ; the northward flux is calculated at the south (and north) face points marked ○ . The face velocities on the tracer cell faces (not shown) will be written as (u**, v**). The grid spacing is denoted by $\Delta\lambda$, $\Delta\phi$ and Δz (each of which can depend on λ, ϕ, z respectively) . The tracer grid points are indexed by integer values of i, j and k in these directions. The variable μ at horizontal location (i,j) is written μ(i,j). The main velocity grid points have half integer indices.

The variables in the vertical (figure 2a) are arranged on a Lorenz grid. The tracers and horizontal velocities are stored together on the same (full) levels and the vertical velocities are stored on intermediate half-levels. The vertical velocities on the u-grid, w^v , are marked ● in figure 2a and those on the tracer grid, w^T , are marked ■ . The w^T are calculated by integrating the horizontal divergence of the main velocities down from the surface. The w^v are calculated similarly except using the face velocities.

(a)

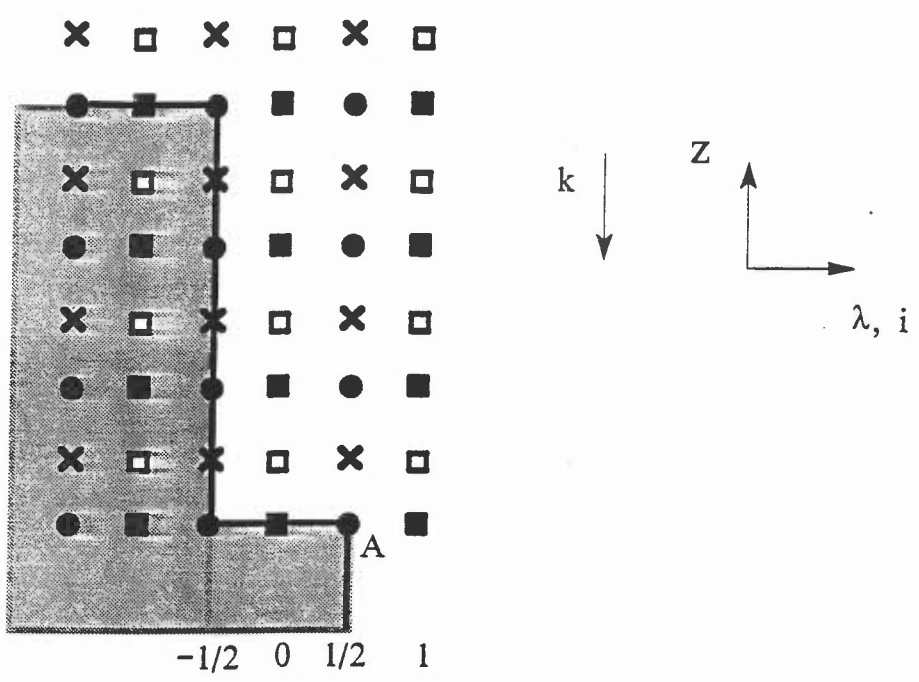

(b)

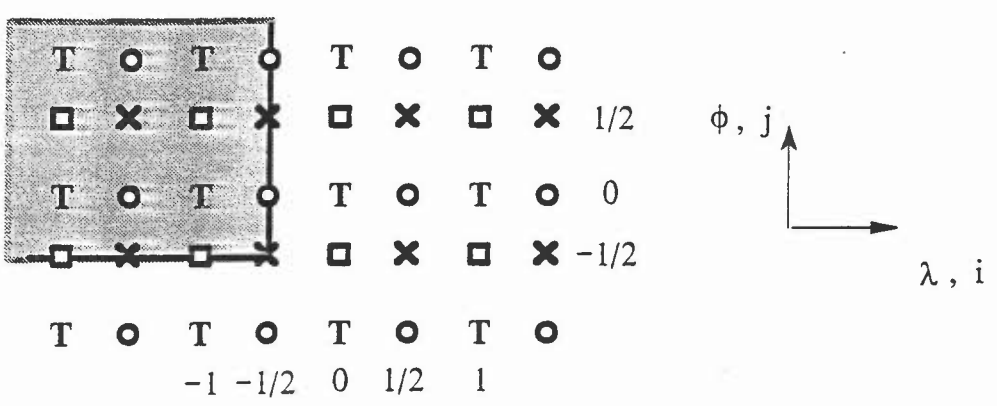

Figure 2: (a) Vertical and (b) horizontal arrangement of variables in the Cox model. Model variables are stored at the points marked as follows: Tracers at T; the main velocities (u,v) at X ; u* at □ ; v* at ○ ; w^v at ● ; w^T at ■ . Representative land boundaries are indicated by solid lines and land points are shaded.

The model represents the ocean's bathymetry by a series of steps; the ocean boundary follows the edges of the cuboid cells with tracer values at their centres (see figure 2a). Viewed from above in the horizontal plane (as in figure 2b), corners of the bathymetry lie on points where the main horizontal velocities are defined. Viewed from the side (as in figure 2a) the horizontal velocities and tracer values lie at the same depths and hence corners in the bathymetry lie at depths mid-way between the velocity values. The corners of the boundary occur at the w^v points (●). Points at or below the boundary of the bathymetry will be termed land points; these points are shaded in figure 2. Throughout this paper no-slip boundary conditions will be assumed. These imply that the total horizontal velocities are zero at land points.

As in the Cox documentation, the barotropic component of the flow will be denoted by a simple overbar (e.g. $\bar{u}$) and the baroclinic component by an overhat (e.g. $\hat{u}$). An overbar followed by an ordinate (λ or ϕ) indicates a centred average over adjacent points in the direction of that variable and centred finite derivatives of μ by $\delta_x \mu$ in which x is the direction; e.g. $(\delta_\lambda \mu)_i = (\mu(i+½) - \mu(i-½)) / \Delta\lambda$. H indicates the depth (at a velocity point), a is the Earth's radius and $m = \sec \phi$. In the standard version of the Cox model the barotropic part is non-divergent and is represented using a streamfunction ψ.

3. Discussion of figure 1

In order to discuss figure 1 in more detail it is helpful at this point to define the standard Cox formulation for the main velocities and the face velocities.

The baroclinic velocities ($\hat{u}^*$, $\hat{v}^*$) at the face points are calculated as centred averages of the adjoining baroclinic velocities ($\hat{u}$, $\hat{v}$) on the main grid:

$$\hat{u}^* = \overline{\hat{u}}^{\lambda} \quad ; \quad \frac{\hat{v}^*}{m} = \overline{\left(\frac{\hat{v}}{m}\right)}^{\phi} \quad . \qquad (1)$$

The barotropic velocities at all sea points are calculated from one streamfunction. The velocities on the main grid are given by:

$$a\, H\bar{u} = -\delta_\phi \overline{\Psi}^{\lambda} \quad ; \quad a\, \frac{H\bar{v}}{m} = \delta_\lambda \overline{\Psi}^{\phi} \quad . \qquad (2)$$

The barotropic velocities for the face velocities are given by:

$$a\, \bar{u}^* = -\delta_\phi \psi \,/\, \max_\lambda(H) \quad ; \quad a\, \frac{\bar{v}^*}{m} = \delta_\lambda \psi \,/\, \max_\phi(H) \quad . \qquad (3)$$

In the standard Cox code the baroclinic velocities and the total velocities on the main grid are **both** set to be identically zero at land points. The important point to note is that by setting the baroclinic velocities at land points to zero the barotropic velocities on the main grid at land

points are **implicitly** set to zero, and hence differ from the values obtained from formula (2) at sea points:

$$\hat{u} = \hat{v} = \bar{u} = \bar{v} = 0 \quad \textit{at land points.} \qquad (4)$$

The large difference in velocity shear at the top of the bathymetry in figure 1a between the flux value (marked by plusses) and the interpolated value (marked by asterisks) from level 9 to level 10 (i.e. from 200 to 300 metres depth) is readily explained. At all levels the contribution to the flux and the interpolated values from the baroclinic velocities is the same. The contribution to the face velocity from the barotropic velocity as given by (3) is also the same at all levels down to level 12. The contribution to the interpolated velocity from the barotropic velocity at the main eastern gridpoint is also independent of depth down to level 12. But the contribution from the barotropic velocity at the western gridpoint is given by (2) from levels 1 to 9 and is zero from the land points at levels 10 and deeper.

This argument shows that the two sets of velocities above steps in the bathymetry will not agree even in the limit as the grid resolution becomes infinite and that the vertical shear in the face velocity at the top of the step will become infinite. In other words the vertical shear in the two sets of velocities is inconsistent at the top of the bathymetric step.

4. Schemes considered

As mentioned earlier scheme A is the one used in the original Cox code, scheme B is simple linear interpolation of values from the main grid to the face points, schemes C and D are new and E is Webb's scheme.

For all schemes the velocities on the tracer grid are unchanged (so the barotropic velocities on the tracer points are given by (2)), the vertical velocity on the tracer grid is determined from the divergence of the fluxes at the faces of the tracer cells,

$$(a/m)\nabla.\boldsymbol{u} = \delta_\lambda(\overline{u\Delta\phi}^{\phi})/\Delta\phi + \delta_\phi(\overline{\frac{v}{m}\Delta\lambda}^{\lambda})/\Delta\lambda \quad , \qquad (5)$$

and the vertical velocity on the velocity grid is determined from the divergence of the fluxes at the faces of the velocity cells,

$$(a/m)\nabla.\boldsymbol{u}^* = \delta_\lambda(u^*) + \delta_\phi(\frac{v^*}{m}) \quad . \qquad (6)$$

A. Cox scheme

This scheme is defined by (1), (3) and (4) above.

B. Simple average of velocities on main grid

This scheme is probably the most obvious choice;

$$u* = \overline{u}^{\lambda} \quad ; \quad \frac{v*}{m} = \overline{\left(\frac{v}{m}\right)}^{\phi} \; . \tag{7}$$

C. Mixed baroclinic/barotropic scheme

In schemes C and D the "barotropic" face velocities are given by:

$$a\,\bar{u}* = -\delta_{\phi}\psi\;\overline{(1/H)}^{\lambda} \quad ; \quad a\,\bar{v}* = \delta_{\lambda}\psi\;\overline{(1/H)}^{\phi} \; . \tag{8}$$

The term "barotropic" is written in inverted commas because, as discussed in section 6.6, the vertical means of the total velocities actually differ from the velocities in (8). The baroclinic velocities on the main grid at land points are taken to be equal but opposite to the barotropic velocities which do not change with depth between land and sea points. The "baroclinic" velocities on the faces for scheme C are given by (1). Note that this implies that at the land points

$$\hat{u}* = -\,\overline{\overline{u}}^{\lambda} \quad ; \quad \left(\frac{\hat{v}*}{m}\right) = -\,\overline{\overline{\left(\frac{v}{m}\right)}}^{\phi} \quad \textit{at land points.} \tag{9}$$

D. Modified Cox scheme

This scheme is the same as scheme C except for the values of the baroclinic velocities on the main grid at land points. If the velocity is being calculated on the face with index 0 and the point on the main velocity grid with index j (where j may be ½ or -½) is a land point the contribution to the "baroclinic" velocity at point 0 from the velocity at point j is taken to be:

$$\begin{aligned} a\,\hat{u}*_{0j} &= \tfrac{1}{2}\,(\delta_{\phi}\psi)_0\;(1/H_j) \\ a\,\frac{\hat{v}*_{0j}}{m} &= -\tfrac{1}{2}\,(\delta_{\lambda}\psi)_0\;(1/H_j) \; . \end{aligned} \tag{10}$$

The form of averaging of H for the "barotropic" velocities in (8) is chosen so that the depth integrated fluxes and bottom vertical velocities have desirable properties.

There is a conceptual difficulty arising at sea points next to the coast which is worth explaining. At velocity face points next to the coast H will be zero at one of the points used in (8) and it

appears that the velocities will be undefined. These face velocity points in the Cox model will lie within the islands and the horizontal derivative of the streamfunction in (8) for any component for which (1/H) is undefined will be identically zero. It is reasonable to take the view that close to the coast (1/H) should not be calculated as a simple two point average - given that 1/H varies rapidly as the coast is approached. The gridbox mean value of 1/H at the velocity point on the coast can be well-defined. By taking the gridbox mean value the barotropic velocity will become well defined and identically zero. In the code itself this conceptual difficulty is deliberately circumvented (without causing errors) by setting 1/H=0 at points where H = 0.

E. Webb's scheme

This scheme uses the fluxes at the faces of the tracer cells to define those at the faces of the velocity cells. The fluxes u**, v** at the faces of the tracer cells are:

$$u^{**}(i+\tfrac{1}{2},j)\,\Delta\phi_{j+\frac{1}{2}} = u(i+\tfrac{1}{2},j-\tfrac{1}{2})\,\Delta\phi_j + u(i+\tfrac{1}{2},j+\tfrac{1}{2})\,\Delta\phi_{j+1} \quad ;$$
$$\frac{v^{**}}{m}(i,j+\tfrac{1}{2})\,\Delta\lambda_{i+\frac{1}{2}} = \frac{v}{m}(i-\tfrac{1}{2},j+\tfrac{1}{2})\,\Delta\lambda_i + \frac{v}{m}(i+\tfrac{1}{2},j+\tfrac{1}{2})\,\Delta\lambda_{i+1} \quad . \qquad (11)$$

The velocities (u*, v*/m) at the velocity cell faces are centred four point averages of these fluxes. For example

$$4u^{*}(i,j+\tfrac{1}{2}) = u^{**}(i+\tfrac{1}{2},j+1) + u^{**}(i+\tfrac{1}{2},j) + u^{**}(i-\tfrac{1}{2},j+1) + u^{**}(i-\tfrac{1}{2},j) \quad . \qquad (12)$$

For a uniform grid spacing this choice ensures that the divergence at the velocity points is the average of the divergence at the four surrounding tracer points.

5. Desirable properties for schemes to calculate face velocities

Properties which might be thought to be desirable are listed here in an order which is convenient for discussion in section 6. The importance of each property is discussed in section 6 at the end of each sub-section.

1. The depth integrated flux of velocity into a velocity cell should be zero. (This is similar to the well known property of the Cox model that the corresponding flux into a tracer cell is zero). When this cannot be established (as is the case for some of the schemes) the scheme should at least be non-divergent for a flow with no variation in one horizontal direction (north, say). Then the depth integrated (eastward) flux should be constant and the same at the velocity face points and the main velocity points.

2. A related property is that w_b, the bottom velocity on the main velocity grid (illustrated by point A on figure 2a) should be related to some finite difference form of $-(\mathbf{u}.\nabla)H$.

3. The calculation of the horizontal and vertical velocity fields from the baroclinic velocities and streamfunction should be at least first order and preferably second order accurate at all points on both grids.

4. A small stencil should be used (or higher than second order accuracy achieved).

5. The scheme should be applicable to a free surface formulation of the model.

6. The baroclinic and barotropic velocities should be clearly separated; the barotropic velocity must be depth independent and dependent only on the streamfunction and the depth mean of the baroclinic velocities must be zero (Killworth et al. 1991 section 3 c provides a discussion of this point).

7. The scheme should be applicable to a barotropic fluid.

6. Derivation and discussion of properties for each scheme

6.1 Non-divergent flux

Ideally the depth integrated flux into the velocity cell with centre point (i,j) =(½, ½) due to u* velocities at (1,½) and (0,½) and v* velocities at (½,0) and (½,1) should sum to zero. This is the case for schemes A, D and E but not for B and C.

The appendix provides derivations of this property for schemes A and D. For Webb's scheme (see (11) & (12)) in the case of a uniform grid the divergence (6) for a velocity cell is the average of the divergence (5) for the four surrounding tracer cells. It is well known that on a grid with uniform latitude and longitude spacing the divergence of the depth integrated flow for tracer cells (as given by (5)) is identically zero:

$$(a/m)\nabla.(H\bar{u}) = \delta_\lambda(\overline{\delta_\phi \overline{\psi}^{\lambda}}^{\phi}) + \delta_\phi(\overline{\delta_\lambda \overline{\psi}^{\phi}}^{\lambda}) = 0. \qquad (13)$$

So the divergence for velocity cells of the depth integrated flow is zero for Webb's scheme.

No corresponding result can be obtained for scheme B for flows which vary with latitude and longitude. This is most easily seen by considering a flat bottom ocean. For this case the sum of the baroclinic velocities over the depth of the fluid is zero. Figure 3 shows the template of tracer points from which the streamfunction makes a contribution to the flux divergence for the velocity cell centred at X. The template has the shape of a Maltese cross. If the streamfunction is non-zero at only one point and that point is one of the outer corners of the cross the flux divergence will be non-zero. So no general results can be obtained. Webb (1995) analyses the vertical velocities which can be obtained for this case in detail.

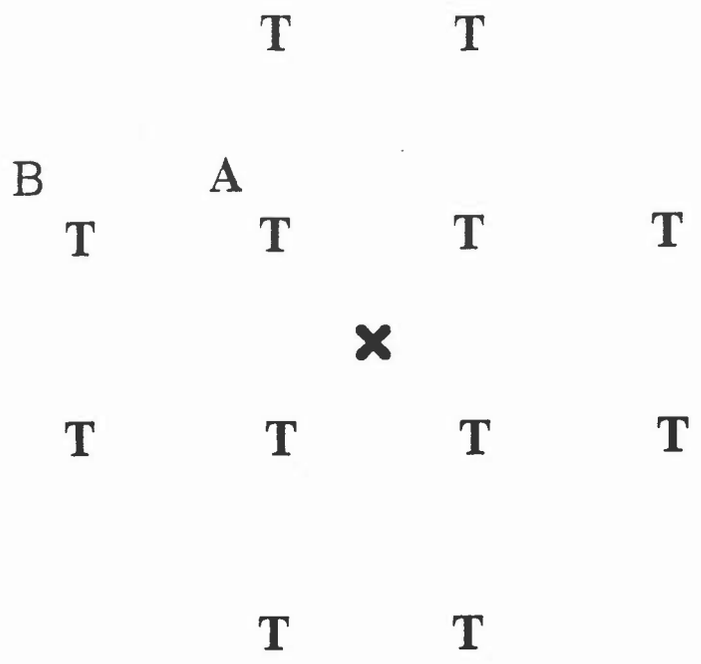

Figure 3: The "Maltese cross" template of streamfunction points used to calculate the vertical velocity at the point marked X. Points A and B are referred to in section 7.2.

The depth integrated transport through the velocity faces can, however, be shown to match that through the main grid points for scheme B in the case of a flow with no variation with latitude. (A similar result holds for flows with no variation with longitude). Suppose that the bathymetry varies with longitude and that the total transport at the main gridpoints $T_u = H\ u\ a\ \delta\phi$ is independent of longitude. Then by (7) the total transport at the velocity face i=0 is given by:

$$T_u(0) = \tfrac{1}{2}T_u(\tfrac{1}{2}) + \tfrac{1}{2}T_u(-\tfrac{1}{2}) = T_u. \qquad (14)$$

For scheme C in the case of a flat bottom ocean the total flux divergence is zero but at bathymetric steps, because the velocities on the main grid are used to determine the baroclinic velocities at land points, the same problem with the template for contributions from the streamfunction arises as for scheme B and no general result can be obtained. For flows with no variation with latitude the depth integrated transport can be shown to be independent of longitude.

The vertical velocities in the rigid lid Cox model are set to zero at the top boundary and integrated down to the bottom using the horizontal flux divergence. The main value of the non-divergent flux property is that it constrains the vertical velocities at the bottom (the corresponding property for the tracer cells guarantees that the vertical velocities at the bottom of the tracer cells are zero). The results in section 8 (table 3) suggest that schemes B and C pay a heavy price for failing to satisfy this property.

6.2 Bottom vertical velocity

As mentioned on page C7 of Cox (1984) the bottom vertical velocity at the velocity points is related to a finite difference form of $-(\mathbf{u}_b.\nabla)H$ where $\mathbf{u}_b$ is the near bottom horizontal velocity.

The appendix derives an expression for the bottom vertical velocity, which will be denoted by w_b , at point A in figure 2a for schemes A and D. To avoid complicated notation, the contribution to w_b evaluated at $i=j=½$ from the zonal velocities is derived for the case when the ocean depth at $(1,½)$ is greater than that at $(0,½)$ (as in figure 2a). With K_i denoting the lowest level which is a sea point at $(i,½)$ the appendix shows that for both schemes A and D

$$(w_b)_{1/2} = - \sum_{k=K_{1/2}+1}^{K_{3/2}} u^*_1 \frac{m}{a} \frac{\Delta z}{\Delta \lambda} \qquad (15)$$

This is of the form $w_b = -(\mathbf{u}_b \cdot \nabla) H$ but with the velocities and bathymetric gradient calculated half a grid square from centre in the direction of the deeper bathymetry and using only velocities below the depth at which w_b is valid. It is clear from the derivations in the appendix that (15) is basically an expression of the conservation of volume in schemes A and D.

Attempts to derive similar results for schemes B and C encounter the same difficulties as in section 6.1. The template of points used by scheme E is wide and it appears that no result involving only the local bathymetry gradient and near bottom currents employed in (15) can be derived. For flows independent of latitude, however, (15) can be derived for schemes B, C and E. The derivation for scheme E is presented as an example in the appendix.

As explained in the introduction, the main reason for requiring well behaved vertical velocities at the bottom of an ocean model is because vortex stretching is important in potential vorticity conservation. It is the bottom vertical velocity on the tracer grid, not the velocity grid, which determines the vortex stretching. (15) is not a centred difference form of $w_b = -(\mathbf{u}_b \cdot \nabla) H$, so schemes A and D may derive little benefit from this property over and above that arising from the non-divergent flux property.

6.3 Accuracy

It is clear that schemes B, C and E for calculating the horizontal velocities at the velocity faces from the baroclinic velocities and streamfunction are centred difference and second order accurate (see e.g. Kreyszig 1982 sections 19.6 & 19.7 for definitions of order of accuracy). The standard scheme for the main velocities is also second order accurate as are the schemes for calculating the two sets of vertical velocities from the horizontal velocities. Thus for these schemes the two sets of horizontal and vertical velocities should agree to second order accuracy.

The barotropic flow for the Cox scheme (see (3)) is not centred difference; only the total transport ($\max_\lambda H)\bar{u}$ is centred difference. Thus the velocities are only accurate to first order

in their treatment of bathymetry. As discussed in section 3, next to bathymetry the velocity shears are not even accurate to first order. Scheme D is centred difference and second order accurate except at points next to bathymetry where it is only first order. Its vertical velocities above bathymetry are second order accurate but adjoining the bathymetry are only first order accurate. (It is worth bearing in mind that in moderately high resolution implementations of the Cox model the bathymetry itself is usually smoothed using a second order accurate filter to enable the model to run with reasonably large timesteps without blowing up (Killworth 1987).)

A problem with scheme C is that at a velocity face which borders land points on both sides, (8) and (9) together can give a non-zero total velocity at points where the bathymetry is varying. In practice this would not affect the model simulation but conceptually one would have to supplement (8) and (9) with a specification that land-locked face velocities are zero. At corners in the bathymetry, scheme E also allows non-zero horizontal velocities at land-locked faces of the velocity cells.

6.4 Spatial extent of stencil

Schemes A and D use the smallest possible stencils to calculate both the baroclinic and barotropic velocities. The stencil for the barotropic velocity in scheme B is larger and for the divergence of the velocities has the form of the Maltese cross shown in figure 3 which is neither small nor compact in shape. The stencil for scheme C is the same as that for D except at points next to steps in the bathymetry where the baroclinic velocities depend on the barotropic velocities calculated as for scheme B. Scheme E calculates each baroclinic face velocity from a 3 x 2 (or 2 x 3) grid of velocities on the main velocity grid. For a rigid lid model, scheme E uses the streamfunction on a 4 x 4 grid to calculate the vertical velocity at a single point on the velocity grid. (The values at the corners of the 4 x 4 grid cancel and so do not in fact contribute.)

There are probably two main advantages of maintaining a small "compact" stencil (there is a technical sense of compact differencing which is not intended to be implied here (see Roache 1976 p 111)). Firstly the coefficient of the leading order term in the truncation error will usually be smaller for the resulting scheme than for a scheme of the same order of accuracy which requires a larger stencil. Secondly only schemes with compact stencils (or derived from schemes using compact stencils) can have desirable properties (such as those derived in sections 6.1 and 6.2).

6.5 Application to free surface formulations

Formulations of the Cox code with a free surface (e.g. Killworth et al. 1991) have several advantages over the rigid lid formulations. They evolve a free surface height field and barotropic velocities but no barotropic streamfunction. Schemes B and E can be used directly with the free surface code with the vertical velocity set at the bottom level and integrated up to the free surface. Schemes C and D reduce to scheme B when they are "extended" to apply to the free surface velocities.

6.6 Separation of baroclinic and barotropic velocities

In scheme A the baroclinic velocities at the face velocities do not depend on the streamfunction and have zero vertical mean and the barotropic flow is independent of depth.

Not all of these statements are true for scheme B. If one takes the view that the baroclinic velocities on the main grid are zero at the land points then the barotropic velocity at the face points is not independent of depth. If one alternatively takes the baroclinic velocities to be equal but opposite to the barotropic velocities at land points, the baroclinic velocities at the face points do not have zero vertical mean. The baroclinic velocities in schemes C and D do not have zero vertical means at face points. The situation for scheme E is the same as that for scheme B.

The face velocities are only used for the advection of momentum in the momentum equation. The division of velocities into baroclinic and barotropic parts on the main grid is necessary to avoid the propagation of short wavelength external gravity waves which result in CFL type instability for all but very short timesteps. These waves propagate in the linearised equations (i.e. with advection of momentum by the flow neglected). There is no reason to suppose that changing the advection of momentum will re-introduce external gravity waves. Thus it is not necessary for the baroclinic and barotropic components of the face velocities to be clearly separated.

6.7 Application to a barotropic fluid

At first sight it may seem that schemes B to E will not apply to barotropic fluids since next to the bathymetry the flow at a given horizontal location will typically vary with depth.

It is reasonable to require that the model represents the flow of a fluid with no density variations (i.e. of a barotropic fluid). If this flow is viscous then it will have boundary layers at the edges of its basin and near the bottom. Thus next to the bathymetry it will vary with depth. Indeed if the flow is viscous it must tend smoothly to zero at its side and bottom boundaries; this is the main motivation for taking the view that the baroclinic flow is equal but opposite to the barotropic flow at land points.

7. Noise in velocity fields

7.1 Due to noise in the streamfunction

Pure gridpoint noise in the streamfunction

$$\psi(i,j) = \Delta\psi(-1)^i(-1)^j \qquad (16)$$

has no influence on the barotropic velocities ($\bar{u}$, $\bar{v}$) on the main grid. This can be seen by substituting (16) into (2). It holds irrespective of variations in the bathymetry H. The velocities (u^*, v^*) on the faces of the velocity cells, as given by (3) and (8) are influenced by gridpoint

noise. An indication of the amplitude, $\Delta\psi$, of noise in the streamfunction which would generate noise of 1 cm/s in the face velocities on a 1° grid ($\Delta y = 10^5$ m) in water of 500 m depth is:

$$\begin{aligned} \Delta\psi &= H\,\Delta u\,\Delta y = 5.10^2\ 10^{-2}\ 10^5\ m^3 s^{-1} \\ &= 5.10^5\ m^3 s^{-1} = 0.5\ Sv. \end{aligned} \tag{17}$$

In regions where the bottom is flat this noise will not affect the vertical velocities. But where the bathymetry is sloping w^v will be affected. When the bathymetry depends only on longitude

$$\begin{aligned} \delta_z \Delta w^v &= \delta_\lambda \overline{(1/H)}^\lambda \frac{\delta_\phi \Delta\psi}{a^2} \\ &= \frac{\Delta H}{H\Delta x}\frac{\Delta\psi}{H\Delta y} \quad . \end{aligned} \tag{18}$$

In the Gulf Stream separation region the bathymetry is very steep and the variation in depth between grid points can be as large as one third of the depth itself. Taking the barotropic velocity across this bathymetry to be as large as 5 cm/s the vertical velocities near the bottom (500 m) due to noise in the streamfunction could be as large as:

$$\begin{aligned} \Delta w^v &= 0.3\ 10^{-5}\ 5.10^{-2}\ 5.10^2\ m\ s^{-1} \\ &= 7.5\ .\ 10^{-3} cm\ s^{-1}\ . \end{aligned} \tag{19}$$

Gridpoint noise in the streamfunction of a few Sverdrup in amplitude is present in the FOAM model. It can be reduced by smoothing the streamfunction using either a Laplacian smoother or the delplus delcross smoother (Killworth et al 1991)

$$\begin{aligned} \Delta\psi(i,j) = a_w\{ &\psi(i,j+1) + \psi(i,j-1) + \psi(i+1,j) \\ &+\psi(i-1,j) - 4\psi(i,j) \\ -\tfrac{1}{2}(&\psi(i+1,j+1) + \psi(i-1,j+1) + \psi(i+1,j-1) \\ &+\psi(i-1,j-1) - 4\ \psi(i,j))\}\ . \end{aligned} \tag{20}$$

This smoothing can be added to the streamfunction provided care is taken to average the increments around island perimeter points (following the code used to solve for the streamfunction) so that the boundary conditions on the streamfunction are not violated.

7.2 Due to noise in the thermal field

Webb (1995) has analysed this source of noise in detail. Assuming thermal wind balance between the tracers and main velocity fields, noise in the face velocities given by (1) can be estimated from noise in the thermal field. By vertical integration of the divergence (6), noise in the vertical velocities w^v can then be estimated.

Pure two grid-length noise in the thermal field (corresponding to (16)) does not affect the main velocities and hence does not affect the face velocities or the w^v. As an alternative to a Fourier analysis of the effect of the thermal field on the velocities (performed by Webb 1995) consider the effect of a temperature field which is non-zero at a single point. Using the thermal wind equation on the main velocity grid:

$$\delta_z u = -\frac{g\alpha}{f} \frac{\delta_\phi \overline{T}^\lambda}{a} \quad . \tag{21}$$

Taking $\alpha = 2\ 10^{-4}\ K^{-1}$, $f = 10^{-4}\ s^{-1}$, $g = 10\ m\ s^{-2}$ and using $\Delta y = a\,\Delta\phi = 10^5$ m and $\Delta z = 600$ m as a depth over which noise in the temperature field may be vertically correlated, noise of 0.01 m/s in the horizontal velocities would be generated by thermal noise of amplitude

$$\Delta T = \frac{10^5}{20} \frac{10^{-2}}{600} K = \frac{1}{12} K \ . \tag{22}$$

For a uniform grid the divergence at the velocity point X in figure 3 due to a non-zero temperature at point A is zero (the fluxes into the box through the north and west faces sum to zero as do the fluxes through the south and east faces). A non-zero temperature at point B provides only a west face flux into the velocity cell surrounding X. Using (21)

$$\Delta w^v = \delta_z w^v \Delta z = -\delta_x u \Delta z = \frac{g\alpha}{f} \frac{\frac{1}{4}\Delta T}{\Delta x\ \Delta y} \Delta z^2 \ . \tag{23}$$

A 1 K thermal increment over a depth of 600 m with $\Delta x = \Delta y = 10^5$ m gives

$$\Delta w^v = 20\ \tfrac{1}{4}\ 10^{-10}\ (600)^2\ m\ s^{-1} = 1.8\ 10^{-2} cms^{-1} \ . \tag{24}$$

Note that this vertical velocity is proportional to $(\Delta z)^2$ i.e. the square of the depth over which thermal "noise" is correlated. By the symmetry of the grid, the magnitude of the velocities at all points on figure 3 equals that at either point A or B.

The above calculations provide a rough but useful guide to the noise which will arise from each source. The results in the next section provide more information on which source of noise is more important in practice.

8. Velocities in test integrations

The statistics presented here are based on velocities which are mean values from the last 30 days of 90 day 1° global integrations started from the Levitus (1982) climatology at rest (Alves et al. 1995). The main integrations differ only in the calculation of the face velocities. For the interpretation of these results the most important aspects of the model physics and parameter

choices are as follows. The bathymetry in the model has been smoothed using two applications of the 2D form of a 1-2-1 filter. The horizontal viscosity is Laplacian with $\nu = 6000$ m^2s^{-1}. Horizontal Laplacian diffusion of tracers with $\kappa = 100$ m^2s^{-1} is augmented by isopycnal diffusion (Redi 1982) as modified by Gerdes et al. (1991) with $\kappa = 2000$ m^2s^{-1} at the surface, $\kappa = 500$ m^2s^{-1} at depth and exponential decay of the difference with a half-depth of 500 m. The original second order advection scheme for momentum and tracers is employed with a one hour time step.

The best way to inspect the velocity fields is to use colour plots of grid square differences. To avoid a plethora of figures I have summarised the results using simple statistical measures for two regions: (a) the "Gulf Stream" region between 25 and 45 °N and 80 and 60 °W and (b) the "Mid-Atlantic" region between 15 and 30 °N and 45 and 25 °W. The first region contains the continental shelf and a strong western boundary current. The second region has weaker currents but includes part of the western side of the Mid-Atlantic ridge.

As noted by Webb the impact of changing the calculation of the face velocities is not particularly dramatic at 1° resolution. The main changes in potential temperatures occur in the regions of the strong boundary currents. Differences in the 30 day mean values between the integrations with schemes A and D are as large as 0.5 °C at 300 m and greater than 0.05 °C up to about 4 gridpoints away from the coast. There are two reasons why the face velocities are not particularly important in this model. Firstly the gridpoint Rossby number is small and non-linear advection plays a minor role in the momentum balance in models at this resolution. Secondly, as noted in the introduction, the vorticity in a B-grid model is naturally defined at the tracer points and it is the vertical velocity at the tracer points which determines the vortex stretching.

A useful consequence of the minor role played by the face velocities is that baroclinic velocity and streamfunction fields calculated by the model using one scheme can be used as input to diagnostic calculations of the face velocities using another scheme without producing misleading results. As it is awkward to implement Webb's scheme fully in the version of the Bryan-Cox model used at the Met. Office (based on Cox 1984), I have estimated vertical velocities for scheme E using output for w^T obtained using scheme A. Webb's scheme has been implemented in MOM 2.0 (Pacanowski 1995) and is likely to be implemented in our model within the next year. The w^T fields in all integrations were similar; only values for w^T obtained using scheme A are displayed.

(a) Horizontal velocities

Table 1 displays statistics for the northward face velocities in the two regions detailed above at 1000 m depth. The velocities for scheme B are simple interpolations of the values on the main grid and are treated as reference values in table 1. The root mean square and maximum absolute values from all gridpoints in the regions are calculated for the fields of differences between the velocities for scheme B and the velocities for schemes A, C and D. The correlation coefficient (r^2) displays the correlations of the velocities for A, C and D with those of scheme B. Results for scheme E are omitted as horizontal velocities for B and E must agree closely.

Table 1: Statistics for monthly mean grid point northern face velocities at 1000 m depth, calculated using different schemes in the Gulf Stream and Mid Atlantic regions (see text for more details). The maximum absolute values and root mean square (RMS) values are calculated using the differences of the velocities from those calculated using scheme B. r^2 is the correlation with the fields calculated using scheme B.

cm/s	Max. abs. value	RMS	r^2
Gulf Stream			
v A	20.5	2.2	0.57
v C	21.7	2.0	0.67
v D	5.8	1.0	0.86
v D sm1	3.7	0.59	0.94
v D sm2	4.3	0.55	0.95
Mid-Atlantic			
v A, C, D	0.68	0.11	0.86
v D sm1	0.22	0.054	0.96
v D sm2	0.25	0.023	0.99

In all cases the velocities only differ appreciably from scheme B at points which are adjacent to land points. In the mid-Atlantic region (which contains no land points at this depth) the results for schemes A, C and D are very similar and quoted together in one row of the table. At the coast schemes A and C provide values which can be very inaccurate (up to 20 cm/s in error). The poor performance of scheme C, despite the fact that it is formally second order accurate, seems to be related to the fact that its velocities at land points may be non-zero (see the last paragraph of section 6.3). At land points below points where B and C differ substantially the velocities implied by scheme C are similar in size to the differences between B and C.

Most of the differences between velocities calculated from B and D can be eliminated by smoothing the streamfunction during the model integration. D sm1 was calculated using a Laplacian smoothing with a coefficient corresponding to $\nu = 6000\ m^2\ s^{-1}$. D sm2 was calculated using the del plus / del cross smoother with $a_w = 0.0016$ which halves grid-scale noise after 50 timesteps (2 days). D sm2, for which the smoothing is more specific to gridpoint noise than D sm1, produces velocities in good agreement with those from scheme B (in which no smoothing

of the streamfunction has been performed). Similar levels of agreement cannot be obtained by such smoothing for schemes A and C: northward velocities calculated for the Gulf Stream region using the output of D sm2 with schemes A and C have correlations r^2 of 0.65 and 0.77 respectively with those from B.

(b) Vertical Velocities

The vertical velocities on the velocity grid, w^v, have been known to disagree with those on the tracer grid for several years (Webb 1995). Webb suggested that this is due to the grid scale noise in w^v which accompanies a purely geostrophic flow over a flat bottom when formulations A-D are used (see section 7.2) . For A, C and D only the baroclinic flow could excite such noise, whilst for B the barotropic flow could also excite this noise. Webb showed that the vertical velocities in the region of the Gulf Stream and the Agulhas current were up to 10 times larger on the velocity grid for the original Cox scheme (i.e. A) than for scheme E.

Table 2 displays the maximum absolute and root mean square values of the monthly average w^v for the same regions as table 1 at 1200 m depth for integrations using schemes A, B, C and D and the integrations with smoothed streamfunction D sm1 and D sm2. Table 2 also presents values for w^v according to Webb's scheme inferred using the w^T from the integration using scheme A. An important point is that the appropriate land/sea mask has been re-imposed on these velocities before calculating the statistics. For schemes A and C very large w^v values can be obtained at land points beneath the Gulf Stream.

Table 2: Statistics for monthly mean grid point vertical velocities at 1200 m depth, calculated using different schemes in the Gulf Stream and Mid-Atlantic regions (see text for more details).

cm/s	Gulf Stream		Mid-Atlantic	
	Max. abs. value	RMS	Max. abs. value	RMS
w^v A	0.048	0.0082	0.0027	0.00063
w^v B	0.071	0.011	0.00093	0.00023
w^v C	0.070	0.0083	0.0028	0.00062
w^v D	0.038	0.0059	0.0028	0.00062
w^v D sm1	0.036	0.0046	0.0041	0.00068
w^v D sm2	0.033	0.0050	0.0037	0.00066
w^v E	0.007	0.0011	0.00042	0.00012
w^T	0.018	0.0022	0.00058	0.00014

In the Gulf Stream region the vertical velocities w^T are somewhat noisy - as can be inferred by comparing them with w^v for scheme E which is simply a four point average of the w^T values. w^v obtained using the schemes A-D has very little correlation with w^v from E; in essence w^v for schemes A-D is dominated by noise. The amplitude of this noise in the Gulf Stream region is largest for scheme B, similar for schemes A and C and smallest for scheme D. For models in which the streamfunction is smoothed the amplitude of w^v in D is just over twice that in w^T.

In the mid-Atlantic at 1200 m schemes A, C and D give similar results. w^v is about 5 times as large as w^T for these schemes and smoothing the streamfunction does not reduce the noise. Remarkably, scheme B produces w^v fields with values comparable to those in w^T (though the correlation between the w^v fields for schemes B and E is negligible; $r^2 = 0.03$).

Table 3 presents results corresponding to those of table 2 but for the bottom vertical velocities, w^v_b. In this table $w^T(I)$ is the vertical velocity at the base of the lowest interior tracer cell (the lowest tracer cell surrounded by sea points on the velocity grid) and is not as simply related to w^v for scheme E as w^T is in table 2. In the Gulf Stream region the w^v_b fields for A-D have almost no correlation with that for E. w^v_b from B and C are particularly noisy. The amplitude of w^v_b in D is about half that in A, but even when the streamfunction is smoothed it is between 3 and 4 times the amplitude of that in E or $w^T(I)$. In the mid-Atlantic region scheme B produces by far the largest w^v_b . The largest w^v_b from scheme D are significantly smaller than those from scheme A (and also scheme C) and have a slightly smaller amplitude than $w^T(I)$. w^v from D sm2 and E have a correlation $r^2 = 0.44$.

Table 3: Statistics for monthly mean grid point bottom vertical velocities, calculated using different schemes in the Gulf Stream and Mid-Atlantic regions (see text for more details).

cm/s	Gulf Stream		Mid-Atlantic	
	Max. abs. value	RMS	Max. abs. value	RMS
w^v A	0.048	0.0098	0.0044	0.00074
w^v B	0.051	0.012	0.0097	0.0020
w^v C	0.147	0.015	0.0044	0.00046
w^v D	0.037	0.0048	0.0023	0.00031
w^v D sm1	0.027	0.0038	0.0015	0.00033
w^v D sm 2	0.035	0.0043	0.0018	0.00031
w^v E	0.015	0.0015	0.0014	0.00022
w^T (I)	0.0064	0.0012	0.0016	0.00038

(c) Discussion of sources of the noise in the vertical velocities

In the Gulf Stream region the thermal field from the model integration is undoubtedly noisy between 300 and 1000 m depths. Subtracting smoothed thermal fields from the fields themselves gives fields which have noise of about 1 K amplitude over the region in which w^v calculated by scheme D is noisy. This noise is strongly correlated in the vertical. Using Δz = 600 m and ΔT = 1 K in (23) gave $\Delta w^v = 1.8\ 10^{-2}$ cm s^{-1} (see (24)) which accords well with the maximum errors found for scheme D. Farrow and Stevens (1995) show that noise in the tracer fields in western boundary currents can be significantly reduced by replacing the second order centred difference formulation for advection used in this model by a third order accurate scheme in which under- and over-shooting of tracer quantities is much reduced.

The model's thermal field between 300 and 1000 m in parts of the Mid-Atlantic region has regular two grid-length noise of about 0.03 K amplitude. This noise appears to be due to the isopycnal diffusion scheme because integrations with increased isopycnal diffusion coefficients show much more vigorous noise. The noise in the tracer fields can be decreased by using the Gent & McWilliams parametrisation of isopycnal thickness diffusion (Gent et al. 1995) or by reducing the isopycnal diffusion or by increasing the horizontal diffusion. This would be likely to reduce the noise in w^v but only to a limited extent. If the noise of 0.03 K amplitude projected perfectly into w^v, (23) suggests its amplitude would be about 5 10^{-4} cm/s but the regular two grid-length thermal noise should project quite poorly into w^v.

Some of the noise in w^v in the Mid-Atlantic region at 1200 m is two grid-length perpendicular to the steps in the bathymetry and of longer scale parallel to the bathymetric steps. This noise increases steadily with depth from 300 to 1200 m and is similar in fields using schemes A, C and D but absent from fields derived using scheme B. It must thus derive from the treatment of the streamfunction. The following argument suggests how barotropic flow over rough bathymetry will generate spuriously large w^v fields for schemes A , C and D but does not explain fully how scheme B avoids them.

The divergence, $\partial w/\partial z$, of the barotropic flow is independent of depth and is given by

$$\partial w/\partial z = \frac{1}{H^2} J(\psi, H) = \frac{1}{H} (\bar{\mathbf{u}}.\nabla H) \quad . \qquad (25)$$

This gives a vertical velocity at the bottom of the model $w_b = -\ \bar{u}.\nabla H$. The actual flow over the bathymetry is typically (i.e. in many areas) much smaller than the barotropic flow; the baroclinic flow at the bottom is almost equal and opposite to the barotropic flow. At 1200 m in the Mid-Atlantic region the vertical velocity due to the divergence of the barotropic flow (25) is larger than that due to the divergence of the full velocity field on the tracer grid at many points and as a consequence is closely anti-correlated with the vertical velocity arising from the divergence of the baroclinic flow above 1200 m. The baroclinic flow is quasi-geostrophic and determined primarily by "thermal wind" balance with the density field. As Webb emphasized the vertical velocity on the tracer grid arising from the baroclinic flow will derive solely from the

ageostrophic part of that flow but the geostrophic part of the flow can "leak" gridscale noise in the geostrophic flow into the vertical velocity on the velocity grid. Because of the stepped bathymetry in the Cox model the vertical velocity due to the barotropic flow reflects the steps in the bathymetry and hence has grid-scale structure. The quasi-geostrophic baroclinic flow to balance this will also have some grid-scale structure and a noisy w^v field.

This extension to Webb's explanation of the origin of noise in the w^v fields strongly suggests that scheme D will not produce good w^v fields unless the bathymetric steps in the model are not constrained to lie at full layer interfaces and the resulting bathymetry is smooth. The latter condition is particularly restrictive and undesirable in regions of steep bathymetry. Given the results in tables 2 and 3, Webb's scheme is clearly to be preferred over scheme D in the FOAM 1° model. The above argument suggests that scheme D is unlikely to give good w^v fields in any model with realistic bathymetry.

9. Conclusions

The method by which the original Bryan-Cox code calculates the horizontal velocities at the faces of velocity cells above bathymetric steps has been shown to produce velocities which are inconsistent with those on the main grid. The manner in which the baroclinic and barotropic velocities are divided leads to large differences at the upper edge of bathymetric steps between the vertical shears in the horizontal velocities at the face points and at the main velocity points. The horizontal fluxes are also sensitive to gridpoint noise in the barotropic streamfunction which is typically present unless the streamfunction is smoothed.

The properties of the original scheme and four alternative formulations are listed in table 4. Scheme A is the original formulation (defined by (1), (3) and (4) in section 3). Scheme B takes the face velocities to be simple averages of the main velocities (see (7)); its main weakness is that its bottom vertical velocities on the velocity grid are non-zero even when the bottom is flat; schemes C and D are similar, the difference between them being that D sacrifices accuracy next to the bathymetry for the sake of the depth integrated flux and bottom vertical velocity. Scheme E due to Webb (see (10) and (11)) takes the face velocities for the velocity cells to be simple averages of the velocities on the faces of the tracer cells. It sacrifices resolution in favour of obtaining two sets of 3D velocities which are internally consistent and vertical velocities which are relatively insensitive to gridpoint noise in the thermal fields.

For free surface models, only B or E are applicable and of these two, as Webb (1995) argued, E is clearly preferable. For rigid lid versions of the model, A and B are poor formulations and should be avoided. C seems to be significantly inferior to D. D provides poor horizontal velocities unless the streamfunction is smoothed appropriately. In the FOAM 1° model the vertical velocities for scheme E are much smaller than those of scheme D. It is argued in section 8(c) that the sensitivity of w^v as calculated by scheme D to noise in the thermal fields which is generated by barotropic flows in regions of steep bathymetry will make Webb's scheme preferable to E in almost any "realistic" Cox model.

Table 4: The properties satisfied by each of the schemes discussed.

Property	original (A)	B	C	D	Webb (E)
zero depth integrated flux	yes	1D case only	1D case only	yes	yes for uniform grid
w_b = - "(u.∇) H"	yes	1D case only; non-zero for flat bottom	1D case only	yes	1D case only
accuracy	1st order in H; inconsistent by steps in H	2nd order	2nd order	1st order in ψ by steps, else 2nd order	2nd order
small stencil	yes	no	except at steps	yes	no
horizontal velocity at land points zero	yes	yes	not adjacent to a step	yes	not at step corners
applicable to free surface code	no	yes	reduce to scheme B		yes
horizontal fluxes sensitive to noise in streamfunction	yes	no	yes	yes	no
w^v sensitive to noise in tracers	yes	yes	yes	yes	no

References

Alves, J. O. S., M. J. Bell, A. L. Cooper, S. J. Foreman, R. M. Forbes, C. G. Sherlock 1995 Performance review of the prototype FOAM system, Forecasting Research Technical Report 159, U K Met. Office.

Arakawa, A., and V. R. Lamb 1977 Computational design of the basic dynamical processes of the UCLA general circulation model. Methods Comput. Phys., 17, 174-256.

Bell, M. J. 1997 Vortex stretching and bottom torques in the Bryan-Cox ocean circulation model. Submitted to J. Geophys. Res. (UKMO Ocean Applications Tech. Note 17).

Bleck, R., and E. P. Chassignet 1994 Simulating the oceanic circulation with isopycnic coordinate models. In The Oceans: Physical-chemical Dynamics and Human Impact. edited by Majumdar S. K., E. W. Miller, G. S. Forbes, R. E. Smalz and A. A. Panah, pp 17-39, Pennsylvania Academy of Science.

Blumberg, A. F., and G. L. Mellor 1987 A description of a three-dimensional coastal ocean circulation model. In Three-dimensional coastal ocean models, Coastal Estuarine Sci., vol 4, edited by N. Heaps, pp 1-16, AGU, Washington, D. C.

Bryan 1969 A numerical model for the study of the circulation of the world ocean. J. Comput. Phys. 4, 347-376

Cox, M. D. 1984 A primitive equation, 3-dimensional model of the ocean. GFDL Ocean Group Tech. Rep. 1, GFDL/NOAA, Princeton.

Farrow, D. E. and D. P. Stevens 1995 A new tracer advection scheme for Bryan and Cox type ocean general circulation models. JPO, 25, 1731-1741.

Gent, P. R., J. willebrand, T. J. McDougall, and J. C. McWilliams 1995 Parametrizing eddy-induced tracer transports in ocean circulation models. J. Phys. Oceanogr. 25, 463-474.

Killworth, P. D. 1987 Topographic instabilities in level model GCMs. Ocean Modellling, 75, 9-12.

Killworth P. D., D. Stainforth and D. J. Webb 1991 The development of a free-surface Byran-Cox-Semtner ocean model. J. Phys. Oceangr. 21, 1333-1348.

Kreyszig, E. 1982 Advanced Engineering Mathematics. Wiley 939 pp.

Levitus, S. 1982: Climatological atlas of the world ocean. NOAA Professional Paper 13.

Pacanowski R. C. 1995 MOM 2.0 Documentation Users' Manual. GFDL Tech. Rep. 3, NOAA/GFDL, Princeton.

Roache, P. J. 1976 Computational Fluid Dynamics. 446 pp. Hermosa Publ., Albuquerque, N. M.

Webb, D. J. 1995 The vertical advection of momentum in Bryan-Cox-Semtner ocean general circulation models. JPO, 25, 3186 - 3194.